Spline-shaped SbD Synthesis of Ogive Radome

M. Salucci, G. Oliveri, M. A. Hannan and A. Massa

Contents

1 [APPROACH 2] Optimization with PSO + Kriging (update negative fitness) - EXP CORRELATION

1.0.1 Motivation and goal

Problem

The main issue encountered when using the PSO+Kriging optimizator is the fact that the optimization end with a negative fitness value, that is not physical.

Solution

In order to overcome such a problem, a different implementation of the optimization algorithm has been taken into account in this section. During the optimization the PSO uses a Kriging predictor to estimate the fitness associated to each trial solution. However, if a negative fitness is predicted for a given particle, the following additional operations are performed:

1. **the particle with negative predicted fitness is simulated** with the full-wave solver;
2. its real fitness is computed and **substituted** to the negative prediction;
3. the particle and its real fitness are **added to the pre-existing training set**, overwriting the training sample with the highest fitness. The dimension of the training set is thus kept constant during the whole optimization process;
4. the Kriging predictor is **re-trained** with the updated training set;
5. the optimization continues, using the updated predictor for successive predictions.

Goal

The mail goal is to avoid the occurrence of negative fitness values during the PSO optimization, since they are not-physical.

1.0.2 Parameters

Optimization targets

- Number of variables: $K = 5$;
- Frequency range:
  - Minimum frequency: $f_{min} = 10.75$ $[GHz]$;
  - Maximum frequency: $f_{max} = 14.5$ $[GHz]$;
  - Number of frequency steps: $N_f = 10$ ($\Delta f \simeq 0.42$ $[GHz]$);
  - Central frequency: $f_0 = \frac{f_{min}+f_{max}}{2} \simeq 12.63$ $[GHz]$;
  - Free-space wavelength at the central frequency: $\lambda_0 = \frac{c}{f_0} = 2.38 \times 10^{-2}$ $[m]$;
- Scanning angle range:
  - Minimum scanning angle: $\theta_{min} = 0$ $[deg]$;
  - Maximum scanning angle: $\theta_{max} = 45$ $[deg]$;
  - Number of angular steps: $N_\theta = 4$ ($\theta_1 = 0$ $[deg]$, $\theta_2 = 15$ $[deg]$, $\theta_3 = 30$ $[deg]$, $\theta_4 = 45$ $[deg]$);

PSO **parameters**

- Population dimension: $P = 10$;
- Maximum number of iterations: $I_{max} = 200$;
- Fitness threshold: $\Phi^{th} = 10^{-20}$;
- Inertial weight: $w = 0.4$;
- Constant inertial velocity;
- Exploration coefficient: $c_1 = 2$;
- Exploitation coefficient: $c_2 = 2$;
- Random seed $s = 1, 2, ..., 10$;
- Initialization (generation of the initial swarm): use the same seed for all the optimizations.

Kriging (Gaussian Process Regressor) parameters

- Regression model: constant (Ordinary Kriging);
- Correlation models:
  - Exponential ($p = 1$);

- Initial guess for hyper-parameters θ_h: $\theta_{h,0} = 0.5$, for $h = 1, ..., K$;
- Lower bound for hyper-parameters θ_h: $min\{\theta_h\} = 0.1$, for $h = 1, ..., K$;
- Upper bound for hyper-parameters θ_h: $max\{\theta_h\} = 20.0$, for $h = 1, ..., K$;

Not-optimized (static) radome parameter

Parameter	Description	Value
L	Length of the radome	1.59×10^{-1} $[m] \simeq 6.69$ λ_0
D	Base diameter of the radome	1.27×10^{-1} $[m] \simeq 5.35$ λ_0
t_0	Thickness of the base and of the top of the radome	$8.20 \times 10^{-3}[m] \simeq \frac{\lambda_r}{2}$
z_1	z-coordinate of the spline control point 1	$\frac{L-t_0}{6}$
z_2	z-coordinate of the spline control point 2	$2\frac{L-t_0}{6}$
z_3	z-coordinate of the spline control point 3	$3\frac{L-t_0}{6}$
z_4	z-coordinate of the spline control point 4	$4\frac{L-t_0}{6}$
z_5	z-coordinate of the spline control point 5	$5\frac{L-t_0}{6}$
ν	External curvature of the radome ($\nu \in [1, 2]$)	1.449 (tangent ogive)
ε_r	Permittivity of the radome material	2.10 (Teflon)
$\tan\delta_r$	Tangent delta of the radome material	$tan\delta = 3.00 \times 10^{-4}$ @ 10.0 $[GHz]$ (Teflon)
λ_r	Wavelength in the radome material	$\lambda_r \simeq \frac{c}{f_0\sqrt{\varepsilon}} \simeq 1.64 \times 10^{-1}$

Table I: List of non-optimized radome parameters.

Antenna Parameters

- Linear dipole array placed over circular ground plane (PEC)
- Number of array elements: $N_e = 8$
- Dipole length: $l_e = \frac{\lambda_0}{2}$
- Array elements spacing: $d_e = \lambda/2$
- Spacing between the array and the ground plane: $h_e = \frac{\lambda_0}{4}$

Parameters boundaries

Parameter	Description	Min	Max
t_1	Radome thickness at the quota $z = z_1$	3.28×10^{-3}[m] ($0.2\lambda_r$)	13.12×10^{-3}[m] ($0.8\lambda_r$)
t_2	Radome thickness at the quota $z = z_2$	3.28×10^{-3}[m] ($0.2\lambda_r$)	13.12×10^{-3}[m] ($0.8\lambda_r$)
t_3	Radome thickness at the quota $z = z_3$	3.28×10^{-3}[m] ($0.2\lambda_r$)	13.12×10^{-3}[m] ($0.8\lambda_r$)
t_4	Radome thickness at the quota $z = z_4$	3.28×10^{-3}[m] ($0.2\lambda_r$)	13.12×10^{-3}[m] ($0.8\lambda_r$)
t_5	Radome thickness at the quota $z = z_5$	3.28×10^{-3}[m] ($0.2\lambda_r$)	13.12×10^{-3}[m] ($0.8\lambda_r$)

Table II: List of all considered boundaries for the optimized radome descriptors.

1.0.3 Comparison between the different random seeds ($s \in [1, 10]$)

Predicted fitness vs. real fitness

Legend

- $\widetilde{\Phi}_0$: Predicted fitness for the best particle of the initial swarm;
- Φ_0: Actual fitness for the best particle of the initial swarm;
- $\widetilde{\Phi}^{opt}$: Predicted fitness for the optimal solution found at the end of the PSO;
- Φ^{opt}: Actual fitness computed for the optimal solution found at the end of the PSO;
- $\Phi^{opt}_{train} = 1.13$: Best fitness inside the training set.

		Predicted		Actual		
Seed	**# Updates**	$\widetilde{\Phi}_0$	$\widetilde{\Phi}^{opt}$	Φ_0	Φ^{opt}	$100\frac{\Phi^{opt}_{train}-\Phi^{opt}}{\Phi^{opt}_{train}}$
1	1	1.13	3.83×10^{-2}	2.11	1.16	-2.65
2	1	1.13	9.51×10^{-3}	2.11	1.47	-30.09
3	2	1.13	1.50×10^{-2}	2.11	1.18	-4.42
4	1	1.13	2.07×10^{-1}	2.11	9.59×10^{-1}	15.13
5	2	1.13	9.84×10^{-3}	2.11	1.09	3.54
6	2	1.13	4.49×10^{-2}	2.11	9.46×10^{-1}	16.28
7	1	1.13	2.43×10^{-2}	2.11	1.52	-34.51
8	**1**	**1.13**	$\mathbf{3.04 \times 10^{-2}}$	**2.11**	$\mathbf{8.48 \times 10^{-1}}$	**24.96**
9	1	1.13	5.99×10^{-2}	2.11	1.14	-0.88
10	1	1.13	1.34×10^{-2}	2.11	1.12	0.88

Table III: Number of updates during the optimization, initial and final predicted fitness and associated real fitness, for each considered random seed $s \in [1, 10]$.

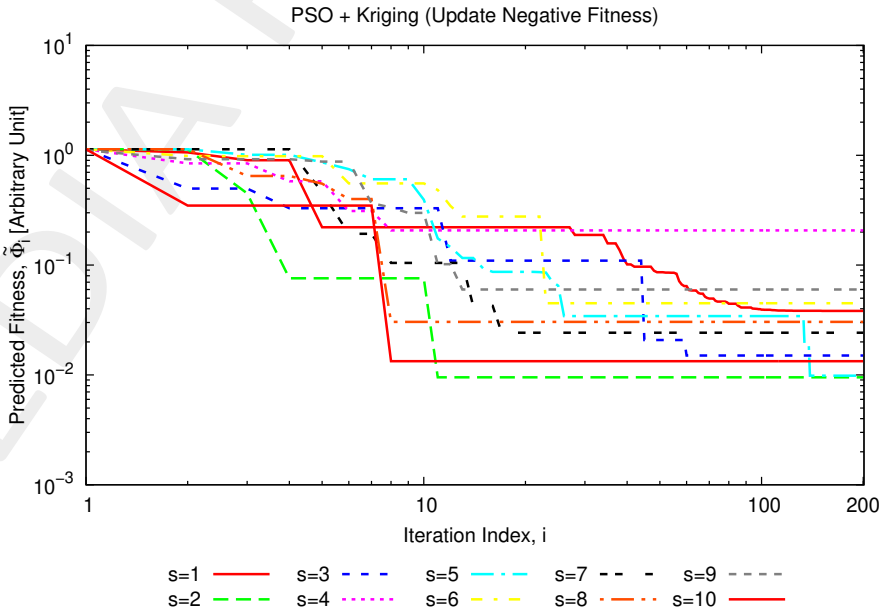

Figure 1: Predicted fitness vs. iteration index, for different random seeds ($s \in [1, 10]$).

Statistics (over $S = 10$ seeds)

Predicted				Actual			
$min\left\{\widetilde{\Phi}^{opt}\right\}$	$max\left\{\widetilde{\Phi}^{opt}\right\}$	$avg\left\{\widetilde{\Phi}^{opt}\right\}$	$std\left\{\widetilde{\Phi}^{opt}\right\}$	$min\left\{\Phi^{opt}\right\}$	$max\left\{\Phi^{opt}\right\}$	$avg\left\{\Phi^{opt}\right\}$	$std\left\{\Phi^{opt}\right\}$
9.51×10^{-3}	2.07×10^{-1}	4.52×10^{-2}	5.61×10^{-2}	8.48×10^{-1}	1.52	1.14	2.04×10^{-1}
Lowest Training Sample							

Table IV: Statistics (min, max, average and standard deviation) of the predicted and actual fitness obtained over $S = 10$ seeds.

1.0.4 Difference between predicted and actual final fitness over $S = 10$ seeds

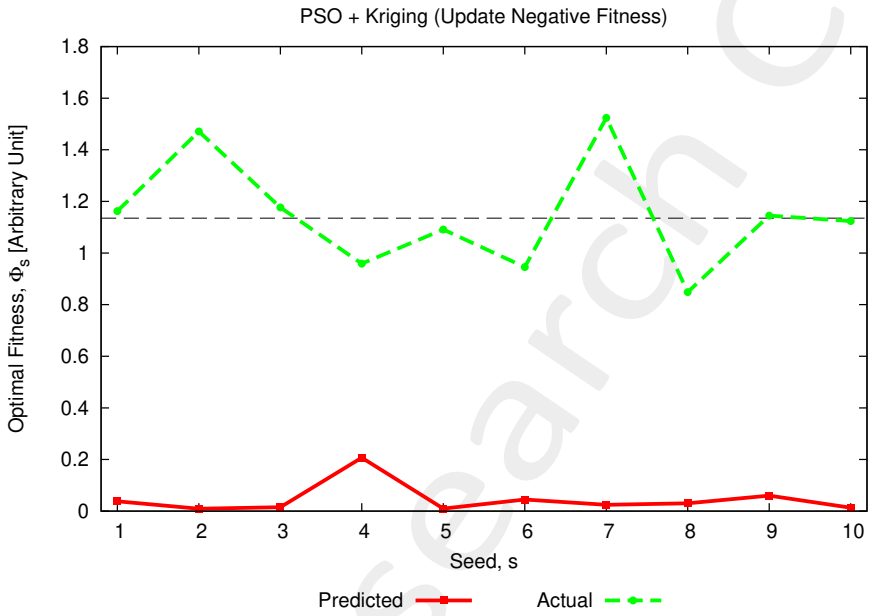

Figure 2: Predicted and actual final fitness for different random seeds ($s \in [1, 10]$).

- Mean Absolute Error (MAE): $MAE = \frac{1}{S}\sum_{s=1}^{S}\left|\widetilde{\Phi}_s^{opt} - \Phi_s^{opt}\right|$
- Normalized Mean Error (NME): $NME = \frac{1}{S}\sum_{s=1}^{S}\frac{\left|\widetilde{\Phi}_s^{opt} - \Phi_s^{opt}\right|}{\left|\Phi_s^{opt}\right|}$
- Matching Error (ME): $ME = \frac{1}{S}\frac{\sum_{s=1}^{S}\left|\widetilde{\Phi}_s^{opt} - \Phi_s^{opt}\right|^2}{\sum_{s=1}^{S}\left|\Phi_s^{opt}\right|^2}$

MAE	NME	ME
1.94	1.39	1.90

Table V: Difference between predicted and actual fitness for all considered random seeds.

1.0.5 Comparison with the PSO that doesn't update the training set (seed $s = 8$)

The following figure directly compares the evolution of the predicted fitness for the same optimal seed ($s = 8$) for

1. the PSO+Kriging updating the negative fitness during the evolution;
2. the PSO+Kriging that does not update the training set during the evolution.

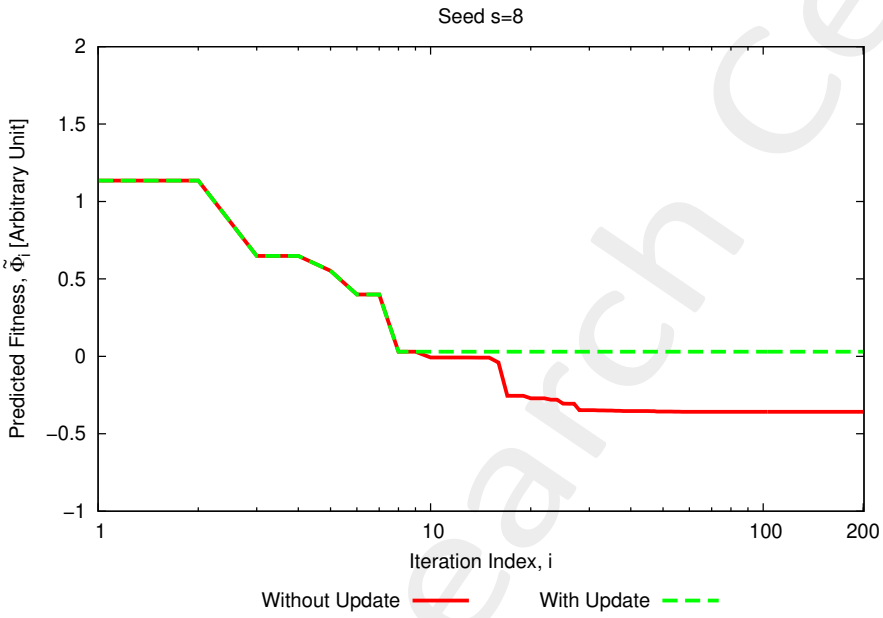

Figure 3: Predicted fitness for seed $s = 8$, when using the two optimization methods (with and without (iteration 1) update of the negative fitness).

As it can be seen, given the same seed and initial swarm, the two fitness curves perfectly overlap up to iteration $i = 8$. This is because at iteration $i = 9$ a negative fitness is predicted for one of the particles in the swarm, and one of the two optimizations continues with an updated training set, while the other one continues with negative fitness values.

1.0.6 Optimized parameters $(t_1^{opt}, ..., t_5^{opt})$ vs. seed

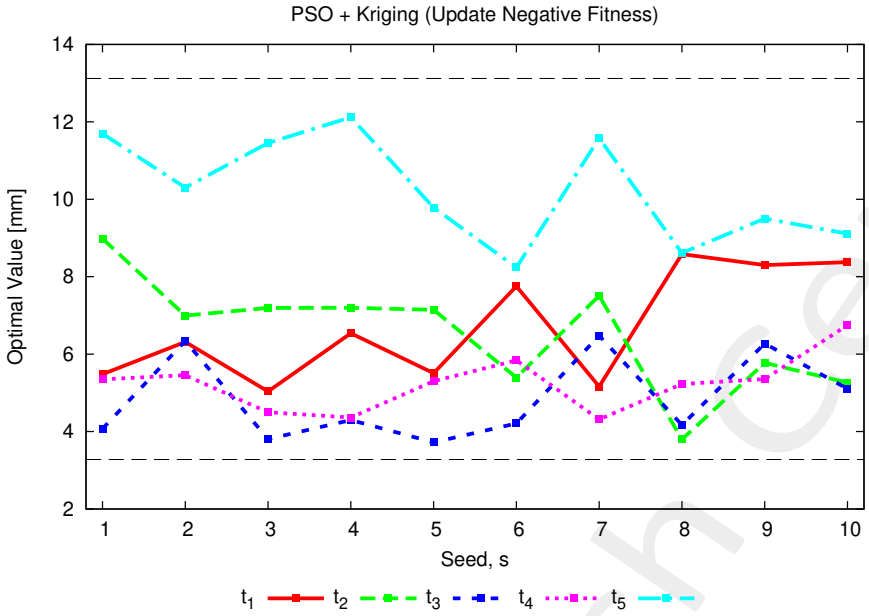

Figure 4: Predicted and actual final fitness for different random seeds ($s \in [1, 10]$).

1.0.7 Best solution found (min. actual fitness)

- Seed: $s = 8$;
- True fitness: $\Phi^{opt} = 8.48 \times 10^{-1}$;
- Average BSE error: $BSE_{avg} = \sqrt{\Phi^{opt}} = 0.92$ [deg].

1.0.8 Analysis of the best solution (seed $s = 8$)

Fitness evolution

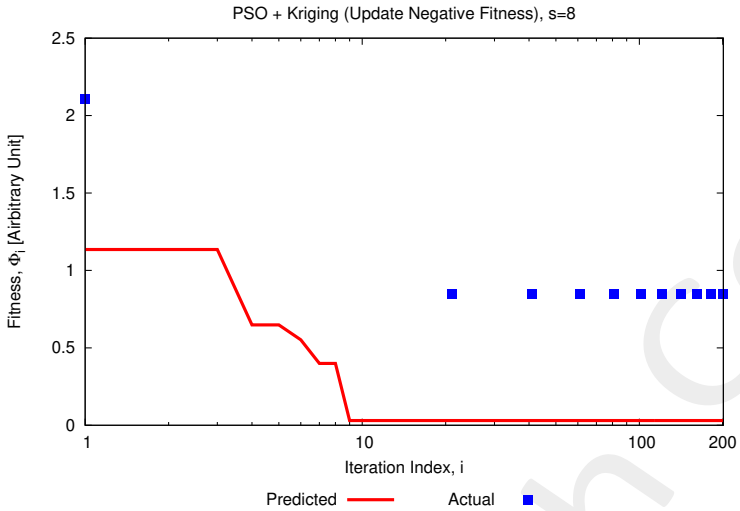

Figure 5: Evolution of the (predicted) fitness and actual fitness computed for the intermediate optimal particles each 20 iterations ("control points").

Optimized parameters $(t_1^{opt}, ..., t_5^{opt})$

Parameter	Description	Optimized Value [m]	Min [m]	Max [m]
t_1	Radome thickness at the quota $z = z_1$	8.58×10^{-3}	3.28×10^{-3}	13.12×10^{-3}
t_2	Radome thickness at the quota $z = z_2$	3.79×10^{-3}	3.28×10^{-3}	13.12×10^{-3}
t_3	Radome thickness at the quota $z = z_3$	4.17×10^{-3}	3.28×10^{-3}	13.12×10^{-3}
t_4	Radome thickness at the quota $z = z_4$	5.23×10^{-3}	3.28×10^{-3}	13.12×10^{-3}
t_5	Radome thickness at the quota $z = z_5$	8.61×10^{-3}	3.28×10^{-3}	13.12×10^{-3}

Table VI: Optimized parameters for the best seed ($s = 8$).

Pointing error (BSE) vs. frequency

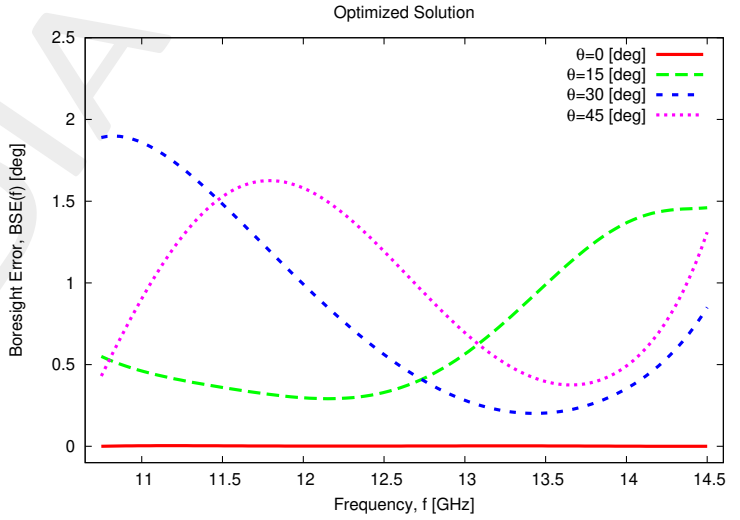

Figure 6: Pointing error (BSE) vs. frequency.

Directivity patterns

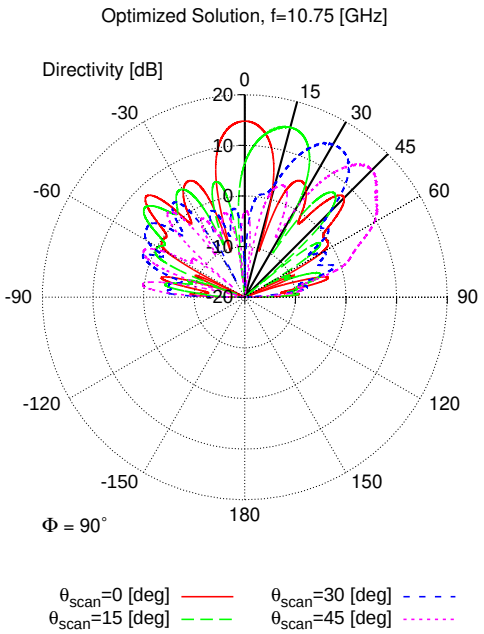

(a) $f = 10.75$ [GHz]

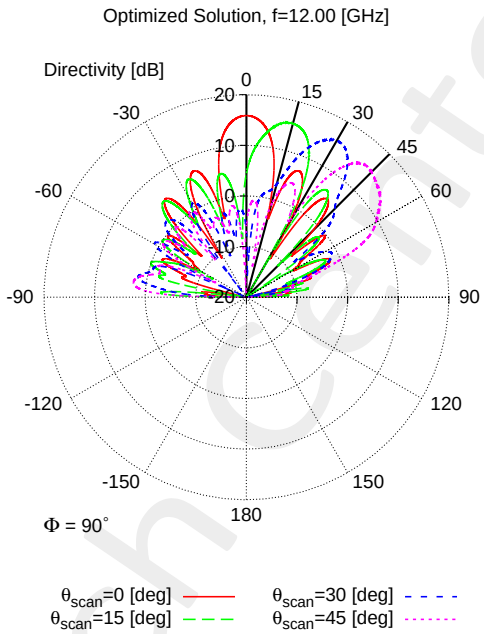

(b) $f = 12.00$ [GHz]

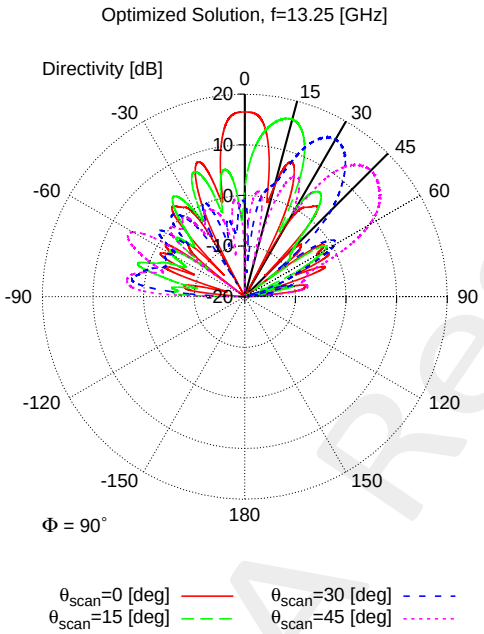

(c) $f = 13.25$ [GHz]

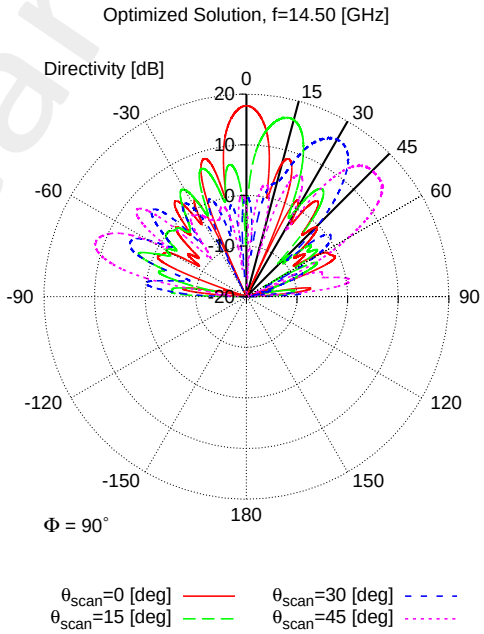

(d) $f = 14.50$ [GHz]

Figure 7: Radiated pattern for the optimized solution at (a) 10.75 [GHz], (b) 12.00 [GHz], (c) 13.25 [GHz] and (d) 14.50 [GHz].

2 [APPROACH 2] Optimization with PSO + Kriging (update negative fitness) - GAUSS CORRELATION

2.0.1 Parameters

Optimization targets

- Number of variables: $K = 5$;
- Frequency range:
  - Minimum frequency: $f_{min} = 10.75$ $[GHz]$;
  - Maximum frequency: $f_{max} = 14.5$ $[GHz]$;
  - Number of frequency steps: $N_f = 10$ ($\Delta f \simeq 0.42$ $[GHz]$);
  - Central frequency: $f_0 = \frac{f_{min}+f_{max}}{2} \simeq 12.63$ $[GHz]$;
  - Free-space wavelength at the central frequency: $\lambda_0 = \frac{c}{f_0} = 2.38 \times 10^{-2}$ $[m]$;
- Scanning angle range:
  - Minimum scanning angle: $\theta_{min} = 0$ $[deg]$;
  - Maximum scanning angle: $\theta_{max} = 45$ $[deg]$;
  - Number of angular steps: $N_\theta = 4$ ($\theta_1 = 0$ $[deg]$, $\theta_2 = 15$ $[deg]$, $\theta_3 = 30$ $[deg]$, $\theta_4 = 45$ $[deg]$);

PSO **parameters**

- Population dimension: $P = 10$;
- Maximum number of iterations: $I_{max} = 200$;
- Fitness threshold: $\Phi^{th} = 10^{-20}$;
- Inertial weight: $w = 0.4$;
- Constant inertial velocity;
- Exploration coefficient: $c_1 = 2$;
- Exploitation coefficient: $c_2 = 2$;
- Random seed $s = 1, 2, ..., 10$;
- Initialization (generation of the initial swarm): use the same seed for all the optimizations.

Kriging (Gaussian Process Regressor) parameters

- Regression model: constant (Ordinary Kriging);

- Correlation models:
  - **Gaussian ($p = 2$);**
- Initial guess for hyper-parameters θ_h: $\theta_{h,0} = 0.5$, for $h = 1, ..., K$;
- Lower bound for hyper-parameters θ_h: $min\{\theta_h\} = 0.1$, for $h = 1, ..., K$;
- Upper bound for hyper-parameters θ_h: $max\{\theta_h\} = 20.0$, for $h = 1, ..., K$;

Not-optimized (static) radome parameter

Parameter	Description	Value
L	Length of the radome	1.59×10^{-1} $[m] \simeq 6.69$ λ_0
D	Base diameter of the radome	1.27×10^{-1} $[m] \simeq 5.35$ λ_0
t_0	Thickness of the base and of the top of the radome	$8.20 \times 10^{-3} [m] \simeq \frac{\lambda_r}{2}$
z_1	z-coordinate of the spline control point 1	$\frac{L-t_0}{6}$
z_2	z-coordinate of the spline control point 2	$2\frac{L-t_0}{6}$
z_3	z-coordinate of the spline control point 3	$3\frac{L-t_0}{6}$
z_4	z-coordinate of the spline control point 4	$4\frac{L-t_0}{6}$
z_5	z-coordinate of the spline control point 5	$5\frac{L-t_0}{6}$
ν	External curvature of the radome ($\nu \in [1, 2]$)	1.449 (tangent ogive)
ε_r	Permittivity of the radome material	2.10 (Teflon)
$\tan\delta_r$	Tangent delta of the radome material	$tan\delta = 3.00 \times 10^{-4}$ @ 10.0 $[GHz]$ (Teflon)
λ_r	Wavelength in the radome material	$\lambda_r \simeq \frac{c}{f_0\sqrt{\varepsilon}} \simeq 1.64 \times 10^{-1}$

Table VII: List of non-optimized radome parameters.

Antenna Parameters

- Linear dipole array placed over circular ground plane (PEC)
- Number of array elements: $N_e = 8$
- Dipole length: $l_e = \frac{\lambda_0}{2}$
- Array elements spacing: $d_e = \lambda/2$
- Spacing between the array and the ground plane: $h_e = \frac{\lambda_0}{4}$

Parameters boundaries

Parameter	Description	Min	Max
t_1	Radome thickness at the quota $z = z_1$	3.28×10^{-3}[m] ($0.2\lambda_r$)	13.12×10^{-3}[m] ($0.8\lambda_r$)
t_2	Radome thickness at the quota $z = z_2$	3.28×10^{-3}[m] ($0.2\lambda_r$)	13.12×10^{-3}[m] ($0.8\lambda_r$)
t_3	Radome thickness at the quota $z = z_3$	3.28×10^{-3}[m] ($0.2\lambda_r$)	13.12×10^{-3}[m] ($0.8\lambda_r$)
t_4	Radome thickness at the quota $z = z_4$	3.28×10^{-3}[m] ($0.2\lambda_r$)	13.12×10^{-3}[m] ($0.8\lambda_r$)
t_5	Radome thickness at the quota $z = z_5$	3.28×10^{-3}[m] ($0.2\lambda_r$)	13.12×10^{-3}[m] ($0.8\lambda_r$)

Table VIII: List of all considered boundaries for the optimized radome descriptors.

2.0.2 Comparison between the different random seeds ($s \in [1, 10]$)

Predicted fitness vs. real fitness

Legend

- $\widetilde{\Phi}_0$: Predicted fitness for the best particle of the initial swarm;
- Φ_0: Actual fitness for the best particle of the initial swarm;
- $\widetilde{\Phi}^{opt}$: Predicted fitness for the optimal solution found at the end of the PSO;
- Φ^{opt}: Actual fitness computed for the optimal solution found at the end of the PSO;
- $\Phi^{opt}_{train} = 1.13$: Best fitness inside the training set.

		Predicted		Actual		
Seed	**# Updates**	$\widetilde{\Phi}_0$	$\widetilde{\Phi}^{opt}$	Φ_0	Φ^{opt}	$100\frac{\Phi^{opt}_{train}-\Phi^{opt}}{\Phi^{opt}_{train}}$
1	1	8.16×10^{-1}	1.08×10^{-2}	1.32	1.37	-21.24
2	1	8.16×10^{-1}	6.18×10^{-1}	1.32	9.79×10^{-1}	13.36
3	1	8.16×10^{-1}	4.21×10^{-2}	1.32	1.08	4.42
4	1	8.16×10^{-1}	1.22×10^{-3}	1.32	1.54	-36.28
5	**1**	$\mathbf{8.16 \times 10^{-1}}$	$\mathbf{1.01 \times 10^{-1}}$	**1.32**	$\mathbf{8.85 \times 10^{-1}}$	21.68
6	1	8.16×10^{-1}	1.63×10^{-1}	1.32	1.09	3.54
7	1	8.16×10^{-1}	6.61×10^{-1}	1.32	1.65	-46.02
8	2	8.16×10^{-1}	1.06×10^{-3}	1.32	9.28×10^{-1}	17.88
9	1	8.16×10^{-1}	6.06×10^{-2}	1.32	9.16×10^{-1}	18.94
10	2	8.16×10^{-1}	3.01×10^{-3}	1.32	1.33	-17.70

Table IX: Number of updates during the optimization, initial and final predicted fitness and associated real fitness, for each considered random seed $s \in [1, 10]$.

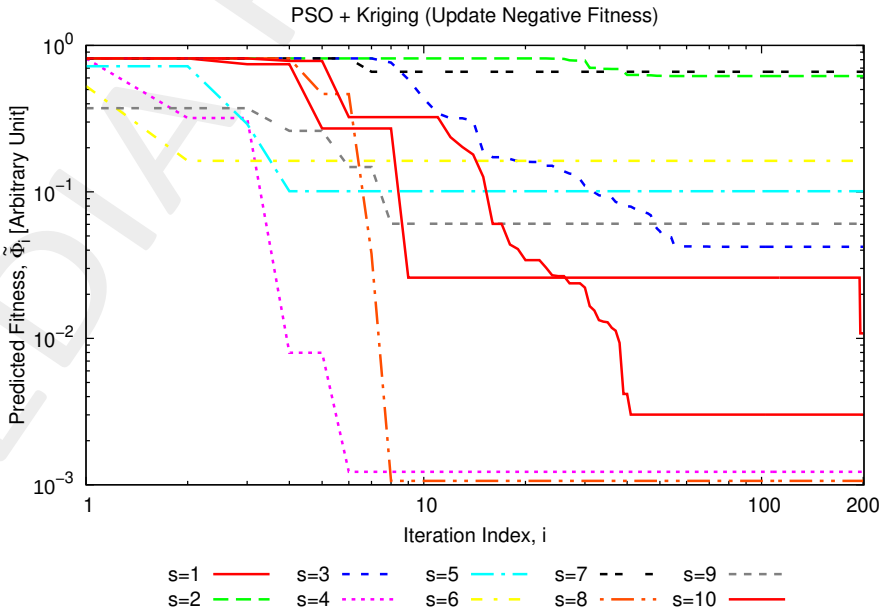

Figure 8: Predicted fitness vs. iteration index, for different random seeds ($s \in [1, 10]$).

Statistics (over $S = 10$ seeds)

Predicted				Actual			
$min\left\{\widetilde{\Phi}^{opt}\right\}$	$max\left\{\widetilde{\Phi}^{opt}\right\}$	$avg\left\{\widetilde{\Phi}^{opt}\right\}$	$std\left\{\widetilde{\Phi}^{opt}\right\}$	$min\left\{\Phi^{opt}\right\}$	$max\left\{\Phi^{opt}\right\}$	$avg\left\{\Phi^{opt}\right\}$	$std\left\{\Phi^{opt}\right\}$
1.06×10^{-3}	6.61×10^{-1}	1.66×10^{-1}	2.42×10^{-1}	8.85×10^{-1}	1.65	1.18	2.61×10^{-1}
Lowest Training Sample							

Table X: Statistics (min, max, average and standard deviation) of the predicted and actual fitness obtained over $S = 10$ seeds.

2.0.3 Difference between predicted and actual final fitness over $S = 10$ seeds

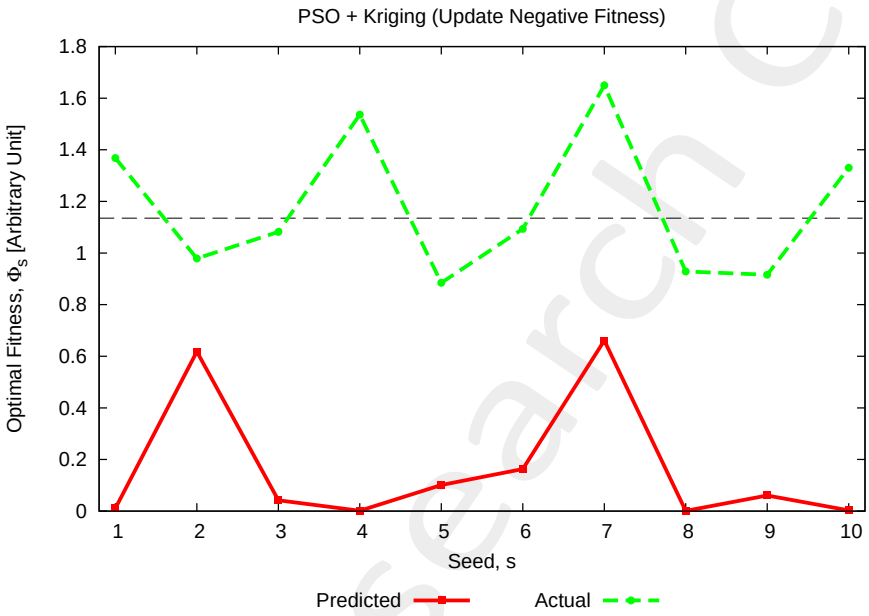

Figure 9: Predicted and actual final fitness for different random seeds ($s \in [1, 10]$).

- Mean Absolute Error (MAE): $MAE = \frac{1}{S}\sum_{s=1}^{S}\left|\widetilde{\Phi}_s^{opt} - \Phi_s^{opt}\right|$
- Normalized Mean Error (NME): $NME = \frac{1}{S}\sum_{s=1}^{S}\frac{\left|\widetilde{\Phi}_s^{opt} - \Phi_s^{opt}\right|}{\left|\Phi_s^{opt}\right|}$
- Matching Error (ME): $ME = \frac{1}{S}\frac{\sum_{s=1}^{S}\left|\widetilde{\Phi}_s^{opt} - \Phi_s^{opt}\right|^2}{\sum_{s=1}^{S}\left|\Phi_s^{opt}\right|^2}$

MAE	NME	ME
1.01	8.59×10^{-1}	7.72×10^{-1}

Table XI: Difference between predicted and actual fitness for all considered random seeds.

2.0.4 Comparison with the PSO that doesn't update the training set (seed $s = 5$)

The following figure directly compares the evolution of the predicted fitness for the same optimal seed ($s = 5$) for

1. the PSO+Kriging updating the negative fitness during the evolution;
2. the PSO+Kriging that does not update the training set during the evolution.

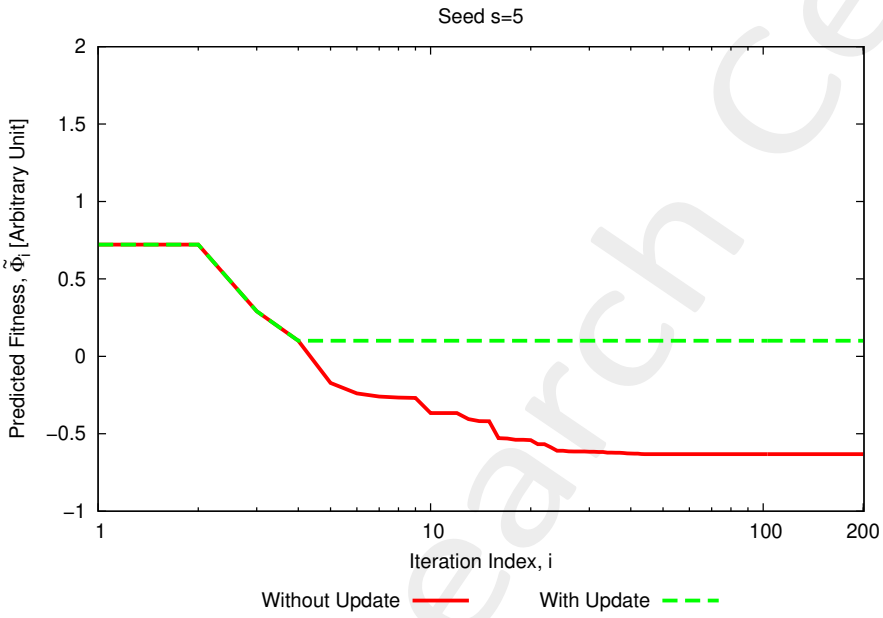

Figure 10: Predicted fitness for seed $s = 5$, when using the two optimization methods (with and without (iteration 1) update of the negative fitness).

As it can be seen, given the same seed and initial swarm, the two fitness curves perfectly overlap up to iteration $i = 5$.

2.0.5 Optimized parameters $(t_1^{opt}, ..., t_5^{opt})$ vs. seed

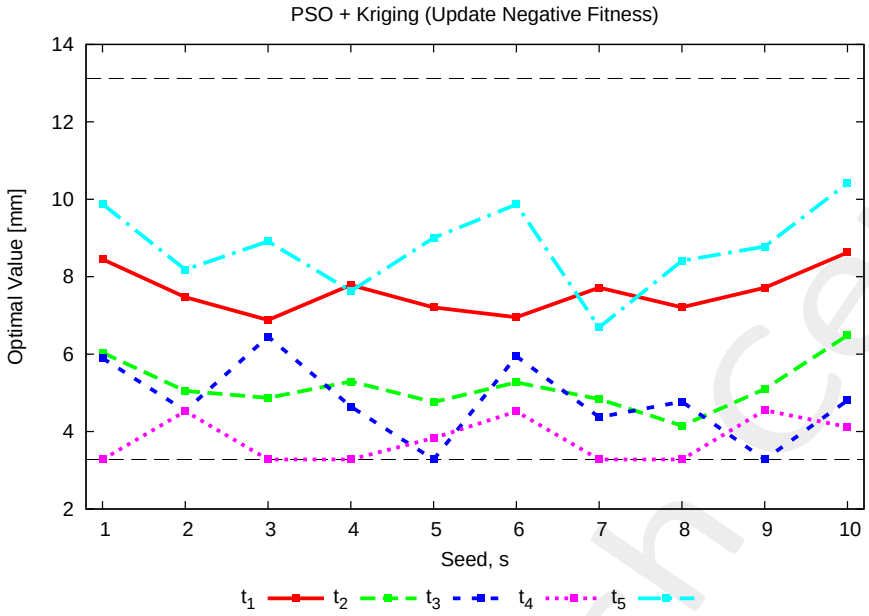

Figure 11: Predicted and actual final fitness for different random seeds ($s \in [1, 10]$).

2.0.6 Best solution found (min. actual fitness)

- Seed: $s = 5$;
- True fitness: $\Phi^{opt} = 8.85 \times 10^{-1}$;
- Average BSE error: $BSE_{avg} = \sqrt{\Phi^{opt}} = 0.94$ [deg].

2.0.7 Analysis of the best solution (seed $s = 5$)

Fitness evolution

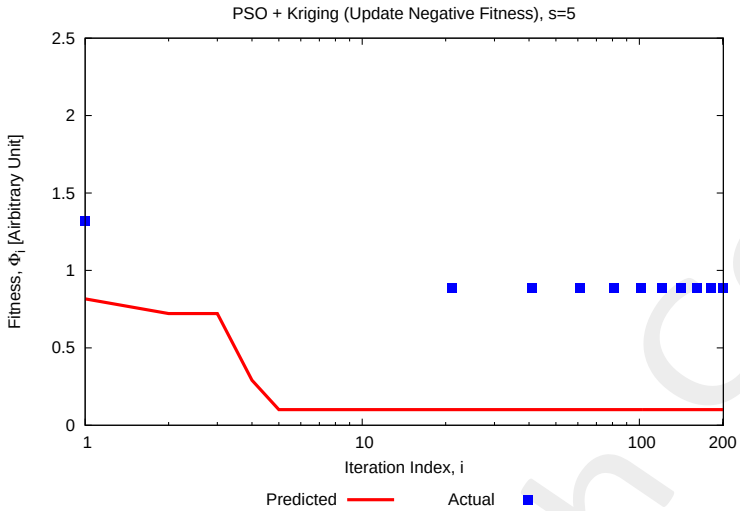

Figure 12: Evolution of the (predicted) fitness and actual fitness computed for the intermediate optimal particles each 20 iterations ("control points").

Optimized parameters $(t_1^{opt}, ..., t_5^{opt})$

Parameter	Description	Optimized Value [m]	Min [m]	Max [m]
t_1	Radome thickness at the quota $z = z_1$	7.21	3.28×10^{-3}	13.12×10^{-3}
t_2	Radome thickness at the quota $z = z_2$	4.76	3.28×10^{-3}	13.12×10^{-3}
t_3	Radome thickness at the quota $z = z_3$	3.28	3.28×10^{-3}	13.12×10^{-3}
t_4	Radome thickness at the quota $z = z_4$	3.83	3.28×10^{-3}	13.12×10^{-3}
t_5	Radome thickness at the quota $z = z_5$	9.00	3.28×10^{-3}	13.12×10^{-3}

Table XII: Optimized parameters for the best seed ($s = 8$).

Pointing error (BSE) **vs. frequency**

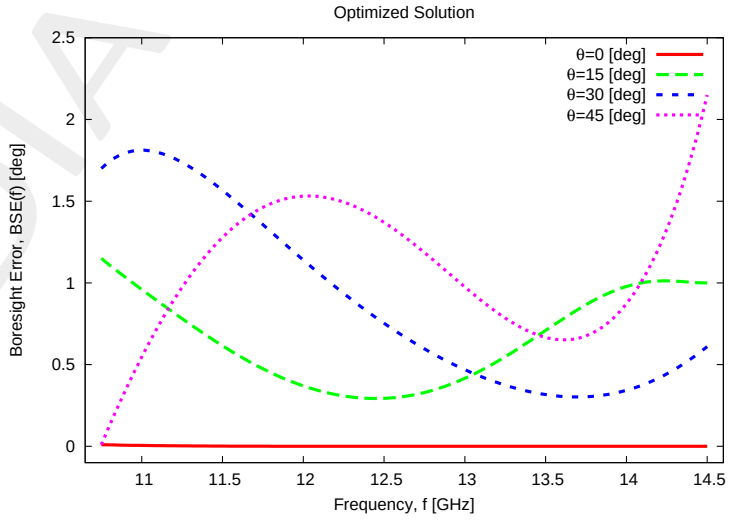

Figure 13: Pointing error (BSE) vs. frequency.

Directivity patterns

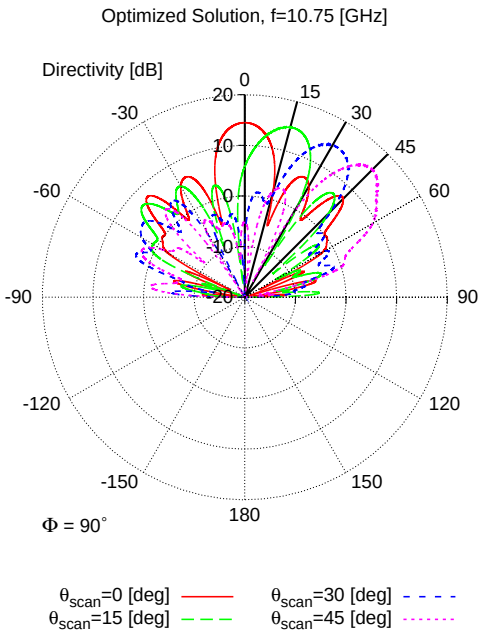

(a) $f = 10.75$ [GHz]

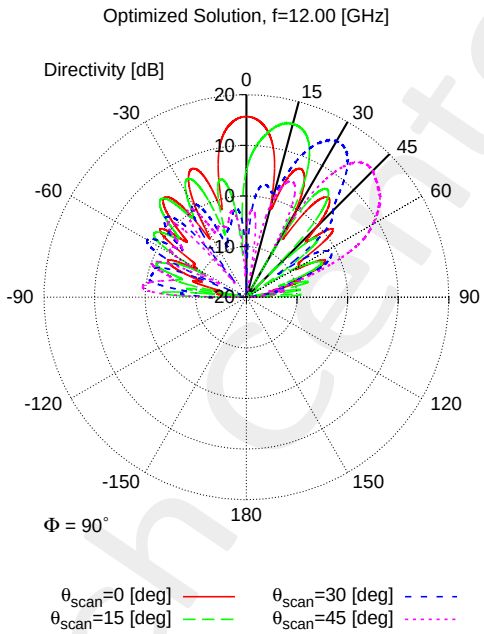

(b) $f = 12.00$ [GHz]

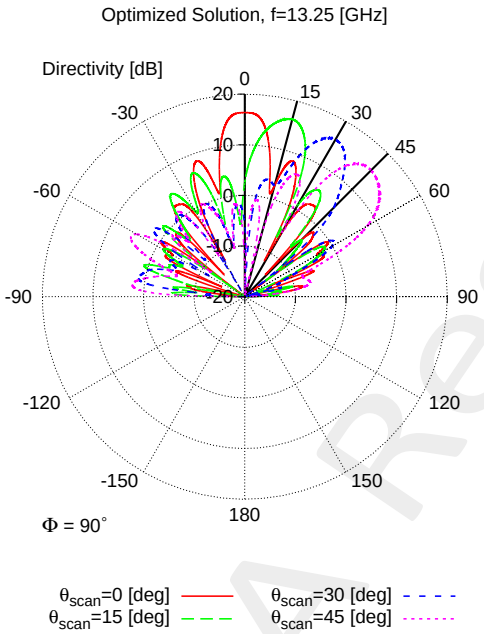

(c) $f = 13.25$ [GHz]

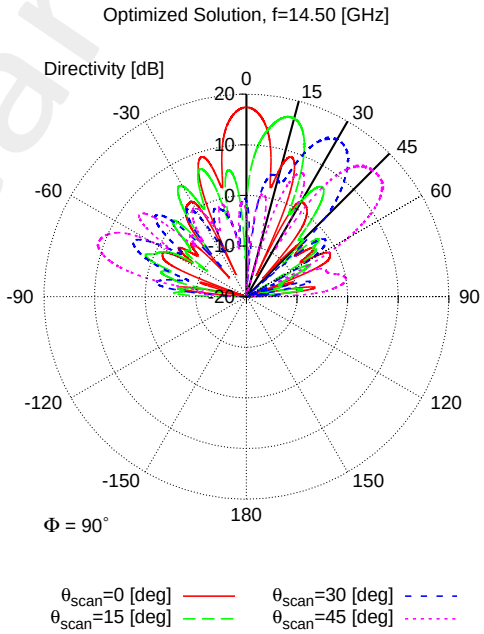

(d) $f = 14.50$ [GHz]

Figure 14: Radiated pattern for the optimized solution at (a) 10.75 [GHz], (b) 12.00 [GHz], (c) 13.25 [GHz] and (d) 14.50 [GHz].

More information on the topics of this document can be found in the following list of references.

References

[1] A. Massa, D. Marcantonio, X. Chen, M. Li, and M. Salucci, "DNNs as applied to electromagnetics, antennas, and propagation - A review," *IEEE Antennas and Wirel. Propag. Lett.,* vol. 18, no. 11, pp. 2225-2229, Nov. 2019.

[2] A. Massa, G. Oliveri, M. Salucci, N. Anselmi, and P. Rocca, "Learning-by-examples techniques as applied to electromagnetics," *Journal of Electromagnetic Waves and Applications, Invited Review Article*, pp. 1-16, 2017.

[3] G. Oliveri, M. Salucci, and A. Massa, "Towards reflectarray digital twins - An EM-driven machine learning perspective," *IEEE Trans. Antennas Propag. - Special Issue on 'Machine Learning in Antenna Design, Modeling, and Measurements*', vol. 70, no. 7, pp. 5078-5093, July 2022.

[4] M. Salucci, L. Tenuti, G. Oliveri, and A. Massa, "Efficient prediction of the EM response of reflectarray antenna elements by an advanced statistical learning method," *IEEE Trans. Antennas Propag.*, vol. 66, no. 8, pp. 3995-4007, Aug. 2018.

[5] M. Salucci, G. Oliveri, M. A. Hannan, and A. Massa, "System-by-design paradigm-based synthesis of complex systems: The case of spline-contoured 3D radomes," *IEEE Antennas and Propagation Magazine - Special Issue on 'Artificial Intelligence in Electromagnetics*,', vol. 64, no. 1, pp. 72-83, Feb. 2022.

[6] G. Oliveri, P. Rocca, M. Salucci, and A. Massa, "Holographic smart EM skins for advanced beam power shaping in next generation wireless environments," *IEEE J. Multiscale Multiphysics Comput. Tech.*, vol. 6, pp. 171-182, Oct. 2021.

[7] G. Oliveri, A. Gelmini, A. Polo, N. Anselmi, and A. Massa, "System-by-design multi-scale synthesis of task-oriented reflectarrays," *IEEE Trans. Antennas Propag.*, vol. 68, no. 4, pp. 2867-2882, Apr. 2020.

[8] M. Salucci, L. Tenuti, G. Gottardi, A. Hannan, and A. Massa, "System-by-design method for efficient linear array miniaturisation through low-complexity isotropic lenses" *Electronic Letters*, vol. 55, no. 8, pp. 433-434, May 2019.

[9] M. Salucci, N. Anselmi, S. Goudos, and A. Massa, "Fast design of multiband fractal antennas through a system-by-design approach for NB-IoT applications," *EURASIP J. Wirel. Commun. Netw.*, vol. 2019, no. 1, pp. 68-83, Mar. 2019.

[10] M. Salucci, G. Oliveri, N. Anselmi, and A. Massa, "Material-by-design synthesis of conformal miniaturized linear phased arrays," *IEEE Access*, vol. 6, pp. 26367-26382, 2018.

[11] M. Salucci, G. Oliveri, N. Anselmi, G. Gottardi, and A. Massa, "Performance enhancement of linear active electronically-scanned arrays by means of MbD-synthesized metalenses," *Journal of Electromagnetic Waves and Applications*, vol. 32, no. 8, pp. 927-955, 2018.

[12] G. Oliveri, M. Salucci, N. Anselmi and A. Massa, "Multiscale System-by-Design synthesis of printed WAIMs for waveguide array enhancement," *IEEE J. Multiscale Multiphysics Computat. Techn.*, vol. 2, pp. 84-96, 2017.

[13] A. Massa and G. Oliveri, "Metamaterial-by-Design: Theory, methods, and applications to communications and sensing - Editorial," *EPJ Applied Metamaterials*, vol. 3, no. E1, pp. 1-3, 2016.

[14] G. Oliveri, F. Viani, N. Anselmi, and A. Massa, "Synthesis of multi-layer WAIM coatings for planar phased arrays within the system-by-design framework," *IEEE Trans. Antennas Propag.*, vol. 63, no. 6, pp. 2482-2496, June 2015.

[15] G. Oliveri, L. Tenuti, E. Bekele, M. Carlin, and A. Massa, "An SbD-QCTO approach to the synthesis of isotropic metamaterial lenses" *IEEE Antennas Wireless Propag. Lett.*, vol. 13, pp. 1783-1786, 2014.

[16] A. Massa, G. Oliveri, P. Rocca, and F. Viani, "System-by-Design: a new paradigm for handling design complexity," *8th European Conference on Antennas Propag. (EuCAP 2014), The Hague, The Netherlands*, pp. 1180-1183, Apr. 6-11, 2014.

[17] P. Rocca, M. Benedetti, M. Donelli, D. Franceschini, and A. Massa, "Evolutionary optimization as applied to inverse problems," *Inverse Problems - 25 th Year Special Issue of Inverse Problems, Invited Topical Review*, vol. 25, pp. 1-41, Dec. 2009.

[18] P. Rocca, G. Oliveri, and A. Massa, "Differential Evolution as applied to electromagnetics," *IEEE Antennas Propag. Mag.*, vol. 53, no. 1, pp. 38-49, Feb. 2011.

[19] P. Rocca, N. Anselmi, A. Polo, and A. Massa, "Pareto-optimal domino-tiling of orthogonal polygon phased arrays," *IEEE Trans. Antennas Propag.*, vol. 70, no. 5, pp. 3329-3342, May 2022.

[20] P. Rocca, N. Anselmi, A. Polo, and A. Massa, "An irregular two-sizes square tiling method for the design of isophoric phased arrays," *IEEE Trans. Antennas Propag.*, vol. 68, no. 6, pp. 4437-4449, Jun. 2020.

[21] P. Rocca, N. Anselmi, A. Polo, and A. Massa, "Modular design of hexagonal phased arrays through diamond tiles," *IEEE Trans. Antennas Propag.*, vol.68, no. 5, pp. 3598-3612, May 2020.

[22] N. Anselmi, L. Poli, P. Rocca, and A. Massa, "Design of simplified array layouts for preliminary experimental testing and validation of large AESAs," *IEEE Trans. Antennas Propag.*, vol. 66, no. 12, pp. 6906-6920, Dec. 2018.

[23] N. Anselmi, P. Rocca, M. Salucci, and A. Massa, "Contiguous phase-clustering in multibeam-on-receive scanning arrays," *IEEE Trans. Antennas Propag.*, vol. 66, no. 11, pp. 5879-5891, Nov. 2018.

[24] G. Oliveri, G. Gottardi, F. Robol, A. Polo, L. Poli, M. Salucci, M. Chuan, C. Massagrande, P. Vinetti, M. Mattivi, R. Lombardi, and A. Massa, "Co-design of unconventional array architectures and antenna elements for 5G base station," *IEEE Trans. Antennas Propag.*, vol. 65, no. 12, pp. 6752-6767, Dec. 2017.

[25] N. Anselmi, P. Rocca, M. Salucci, and A. Massa, "Irregular phased array tiling by means of analytic schemata-driven optimization," *IEEE Trans. Antennas Propag.*, vol. 65, no. 9, pp. 4495-4510, Sept. 2017.

[26] N. Anselmi, P. Rocca, M. Salucci, and A. Massa, "Optimization of excitation tolerances for robust beamforming in linear arrays" *IET Microwaves, Antennas & Propagation*, vol. 10, no. 2, pp. 208-214, 2016.

[27] P. Rocca, R. J. Mailloux, and G. Toso, "GA-Based optimization of irregular sub-array layouts for wideband phased arrays desig," *IEEE Antennas and Wireless Propag. Lett.*, vol. 14, pp. 131-134, 2015.

[28] P. Rocca, M. Donelli, G. Oliveri, F. Viani, and A. Massa, "Reconfigurable sum-difference pattern by means of parasitic elements for forward-looking monopulse radar," *IET Radar, Sonar & Navigation*, vol 7, no. 7, pp. 747-754, 2013.

[29] P. Rocca, L. Manica, and A. Massa, "Ant colony based hybrid approach for optimal compromise sum-difference patterns synthesis," *Microwave Opt. Technol. Lett.*, vol. 52, no. 1, pp. 128-132, Jan. 2010.

[30] P. Rocca, L. Manica, and A. Massa, "An improved excitation matching method based on an ant colony optimization for suboptimal-free clustering in sum-difference compromise synthesis," *IEEE Trans. Antennas Propag.*, vol. 57, no. 8, pp. 2297-2306, Aug. 2009.

[31] N. Anselmi, L. Poli, P. Rocca, and A. Massa, "Design of simplified array layouts for preliminary experimental testing and validation of large AESAs," *IEEE Trans. Antennas Propag.*, vol. 66, no. 12, pp. 6906-6920, Dec. 2018.

[32] M. Salucci, F. Robol, N. Anselmi, M. A. Hannan, P. Rocca, G. Oliveri, M. Donelli, and A. Massa, "S-Band spline-shaped aperture-stacked patch antenna for air traffic control applications," *IEEE Trans. Antennas Propag.*, vol. 66, no. 8, pp. 4292-4297, Aug. 2018.

[33] F. Viani, F. Robol, M. Salucci, and R. Azaro, "Automatic EMI filter design through particle swarm optimization," *IEEE Trans. Electromagnet. Compat.*, vol. 59, no. 4, pp. 1079-1094, Aug. 2017.